INTERNATIONAL ATOMIC ENERGY AGENCY
UNITED NATIONS EDUCATIONAL, SCIENTIFIC AND CULTURAL ORGANIZATION

INTERNATIONAL CENTRE FOR THEORETICAL PHYSICS
34100 TRIESTE (ITALY) - P.O.B. 586 - MIRAMARE - STRADA COSTIERA 11 - TELEPHONE: 2240-1
CABLE: CENTRATOM - TELEX 460892-I

SMR/389 - 8

WORKING PARTY ON
MODELLING THERMOMECHANICAL BEHAVIOUR OF MATERIALS
(29 May - 16 June 1989)

A SIMPLE DISLOCATION MODEL FOR HIGH TEMPERATURE DEFORMATION

J.R. MATTHEWS
Aere Harwell
Theoretical Physics Division
Oxon OX11 ORA
Didcot
United Kingdom

These are preliminary lecture notes, intended only for distribution to participants.

A Simple Dislocation Model for High Temperature Deformation

J.R. Matthews

Abstract

The advantages of including a simple microstructural description in phenomenological creep laws are described. A simple model is built up in stages to illustrate how the main features of the high temperature deformation can be reproduced. The model is extended to include the effects of irradiation and made compatible with current theories of radiation damage, irradiation creep and neutron induced voidage swelling. The main examples are taken from austenitic stainless steel.

Theoretical Physics Division
AERE Harwell

January, 1985

HL85/1056 (C15)

CONTENTS

TABLE

ILLUSTRATIONS

ISBN 0-7058-1330-4

CONTENTS (cont'd)

ILLUSTRATIONS (cont'd)

List of Symbols

b	Magnitude of dislocation Burger's vector.
c_1	Proportion of dislocation links acting as forced climb sources.
c_2	Constant governing forced climb assisted recovery.
c_j	Jog concentration.
d	Sub-grain boundary diameter.
h_1	Distance moved by dislocation link per activated event.
h_2	Pinning spacing of dislocations.
k	Boltzmann's constant.
L	Mean free path of dislocations.
s	Size parameter controlling absorption of point defects at dislocations.
T	Absolute temperature
U_m	Activation energy for dislocation link unpinning.
v	Mean dislocation velocity, climb or glide.
v_c	Dislocation climb rate driven by internal stresses.
v_ϕ	Dislocation climb rate forced by point defect irradiation induced point defect supersaturation.
α	Constant governing internal stress generated by dislocation network.
β	Constant governing scale of sub-grain formation.
δ	Maximum separation of dislocations for spontaneous recovery.
ϵ	Plastic strain.
η	Proportion of dislocation links acting as sources.
μ	Shear modulus.
ν	Attempt frequency for link unpinning.
ρ	Dislocation density.
σ	Applied stress.
σ_1	Local stress on dislocations from line tension or pile-ups.
σ_2	Long range internal stress from dislocation network.
σ_o	Flow stress for dislocation links.
σ_ϕ	Virtual stress arising from irradition effects.
Ω	Atomic volume.

1. Introduction

A good representation of creep deformation is an essential part of the design and assessment of nuclear fuel pin behaviour. This is particularly so for the cladding of fast reactor fuel pins, which is subjected to a wide range of stresses during normal operations and during testing for behaviour in hypothetical accidents. The difficulties in collecting and interpreting high temperature deformation data has meant that most creep design of components has been done using simple steady-state creep correlations. It has long been recognised that primary creep is important and cold-worked materials often have persistent transient behaviour and no proper steady-state is reached. To resolve this difficulty tests are often conducted using stress or temperature ramps that try to mimic the conditions predicted during operation or in off-normal situations[1,2]. More detailed descriptions are required for the calculation of pellet-clad interactions in reactor fuel pins during power changes or the more severe conditions during an accident.

Complicated phenomenological deformation models have been constructed for Zircaloy and 316 stainless steel with some success[3,5]. The construction of these models required the fitting of a large number of free parameters; over 40 for the austenitic stainless steel model. Despite this the models are valid only for a particular cast of materials and do not fit the data well in some conditions. There are a number of advantages in introducing a microstructural element into such phenomenological theories, even if a truly microstructural description is not attainable:

(i) The expressions are simpler, because many of the free parameters may be eliminated in terms of physical properties such as elastic constants, lattice parameters and diffusion coefficients etc.;

(ii) Observable quantities may also be calculated, providing extra confidence in the predictions and warning of changes in mechanisms;

(iii) Speculation on the effect of changing the metallurgical state of material is possible;

(iv) The theory may be extended into new regimes such as accounting for the effect of radiation damage.

This report describes how such a phenomenological model of high temperature deformation incorporating a simple microstructural description can be constructed. It uses as its basis concepts which have proved efficacious in describing radiation effects in metals; i.e. chemical rate theory[6]. Some progress has already been made in using the rate theory to describe thermal creep and the effect of irradiation creep where dislocation climb dominates dislocation multiplication and recovery and is also responsible for the macroscopic strain[7,8]. This work looks at a wider range of stress conditions where dislocation glide may also be important. Only isotropic deformation is described in terms of a single representative dislocation system. The question of how the multiple dislocation systems interact with one another and response to multi-axial stress states will be left to a future paper. A paper dealing with a fuller microstructural model will be published separately[9].

2. The Basic Model - Hardening vs. Recovery

The basis for the model is not original. We use the simple concept of a competition between work hardening and recovery controlling the dislocation density in the material and also the internal stress state which modifies the

driving force for dislocation motion[10,12]. Two rate equations govern the deformation and the dislocation density:

$$\dot{\varepsilon} = b\rho v \tag{1}$$

which is often known as the Orowan equation and relates the strain produced by dislocations to their movement; and

$$\dot{\rho} = \frac{\dot{\varepsilon}}{bL} - 2\rho^{\frac{1}{2}} v_c - \frac{\delta\rho\dot{\varepsilon}}{b} \tag{2}$$

which governs the balance between dislocation multiplication and recovery by two distinct processes. The right hand side of equation (2) is made up of three terms which are respectively: the dislocation multiplication term which is simply a re-statement of the Orowan equation; a climb recovery term; and a dynamic recovery term where dislocations spontaneously slip to annihilate if they come within a distance δ of each other. In a form with only the first two of these terms equation (2) has been frequently used to derive creep equations[13]. Often the dislocation density is identified with an internal stress opposing motion with the applied stress and when a stable dislocation density is attained a steady-state creep expression may be derived[14]. Equations (1) and (2) were probably first used in a phenomenological theory for micro-plasticity by Johnson and Gilman[15] and an expression with all three terms in equation (2) was used by Webster in his assessment of primary creep[16].

Before trying to define a high temperature deformation law using equations (1) and (2) let us concentrate on the significance of the two parameters L and δ. We can do this by studying the behaviour of equation (2) when the strain rate is sufficiently high for climb recovery to be insignificant:

$$\dot{\rho} = \frac{\dot{\varepsilon}}{bL} - \frac{\delta\rho\dot{\varepsilon}}{b} \quad . \tag{3}$$

If the applied stress is well above the flow stress of the material, dislocations will be generated at a rate which is determined by the opposing internal stress from the existing dislocation network. This will be discussed in more detail when the dislocation velocity is dealt with. We might therefore expect a relationship between the applied stress and the dislocation density of the form:

$$\sigma = \sigma_o + \alpha b\mu \rho^{\frac{1}{2}}, \tag{4}$$

where σ_o is the flow stress of the dislocations and α is a constant between 0.5 and 1. In stainless steels σ_o is controlled by solute hardening and will be a function of temperature and the metallurgical state of the steel. If the mean free path of the dislocations is initially fixed by precipitates or in a well annealed pure material by the grain size then the solution of equation (3) will give parabolic hardening:

$$\sigma = \sigma_o + \alpha\mu\,(b\varepsilon/L)^{\frac{1}{2}} \quad . \tag{5}$$

As strain is accummulated the dislocation network size will become smaller than the initial value of the mean free path and this will then become a function of dislocation density:

$$L = 1/(\beta\rho^{\frac{1}{2}}) \quad , \tag{6}$$

and the strain hardening will become linear. In materials without precipitates and the dislocation network dominates the solution of equation (2) gives the Voce hardening relationship[18]:

$$\sigma = \sigma_o + (\beta\alpha\mu b/\delta)[1 - \exp(-\beta\delta\varepsilon/2b)] \, . \tag{7}$$

The stress-strain relationship implied by this model is illustrated in Fig.1. This behaviour is typical of polycrystalline metals and alloys and high strain rate data can help us fix the correct values for α, δ and the

initial size of L. We might expect that the value of σ is related to the flow stress of the material, as the critical distance for spontaneous glide of dislocations towards one another will be controlled by their mutual interaction stress. Experimental observations of this saturation at temperatures below those where climb recovery is expected to be important imply a relationship:

$$\delta \simeq 0.25\beta\mu b/\sigma_o . \tag{8}$$

The spacing δ will therefore increase with temperature as σ_o decreases.

The climb recovery term in equation (2) represents the simplest model of this process. It is based on the network recovery model of Friedel[19]. The mean climb velocity is given by:

$$v_c = D_s \frac{\Omega\mu}{kT} \rho^{\frac{1}{2}} \frac{b}{s} , \tag{9}$$

where s is a scale parameter controlling the absorption of point defects by dislocations which is equal to the spacing of jogs when climb is jog limited. When climb is sink limited, which will be the case at high temperatures, high strain rates or during irradiation, s is a weak function of the dislocation density. This recovery model is useful as a basis for deformation models but in practice recovery is a complex process. The same driving forces for dislocation annihilation are also responsible for sub-grain formation. The pinning of dislocations by precipitates can inhibit recovery and reduction of the dislocation density is limited unless recrystallisation takes place. This will be discussed further.

3. Creep at High and Low Stresses

One problem with existing models of high temperature deformation is that they try in a single model to cover the entire stress and temperature range. Recognition that more than one mechanism may be operating can greatly simplify correlations used to fit experimental data and eliminate some of the more contrived models. It is proposed here that four creep regimes are sufficient to explain most observations. For high temperature deformation at very low stress levels simple diffusive creep may occur and this has now been demonstrated for materials which had previously been assumed to be resistant to it. For stresses below the dislocation flow stress a dislocation creep mechanism based on either a climb-creep model[8,20] or viscous motion of the dislocations is suggested[19]. Above the dislocation flow stress, strain is generated by gliding dislocations and controlled by a combination of the internal stress generated by the network and the activated cutting of obstacles. At the highest stresses the behaviour is dominated by dynamic recovery processes.

A discussion of the details of Coble and Nabarro-Herring creep is outside the scope of this paper, so let us first look at the characteristics of the dislocation climb creep model. Strain is generated by climbing dislocation edge segments and dislocation multiplication is by the operation of climb sources. We may safely assume that the dislocation densities are low enough for dynamic recovery processes to be unimportant. The dislocation velocity is[9]:

$$v = (D_s/s) \{\exp[(\sigma - \alpha\mu b\rho^{\frac{1}{2}}) \Omega/kT] - 1\}$$

$$\simeq (D_s/s) (\sigma - \alpha\mu b\rho^{\frac{1}{2}}) \Omega/kT. \tag{10}$$

Equations (1) and (2) become for the case where the mean free path of the dislocations is determined by the network spacing:

$$\dot{\varepsilon} = \rho D_s (b/s) (\sigma - \alpha \mu b \rho^{\frac{1}{2}}) \Omega/kT \tag{11}$$

and

$$\dot{\rho} = 2\rho^{\frac{1}{2}} \frac{\dot{\varepsilon}}{b} - 2\rho^2 D_s \frac{b \mu \Omega}{s k T} . \tag{12}$$

This is a gross simplification of the climb creep model presented earlier, but has all the principal features except that the separate build-up of dislocation populations of different orientations cannot be modelled. Very similar expressions for dislocation velocity can be found for solute drag where the dislocation velocity is controlled by either the self diffusion or solute diffusion coefficient[19,21].

Equations (11) and (12) describe the transient creep behaviour and we can obtain a steady-state law by making $\dot{\rho}=o$. We find:

$$\sigma = (1 + \alpha) \mu b \rho^{\frac{1}{2}} \tag{13}$$

and

$$\dot{\varepsilon} = 2D_s \frac{\Omega \mu}{bs kT} \left(\frac{\sigma}{(1 + \alpha)\mu} \right)^3 . \tag{14}$$

For stresses above the dislocation flow stress dislocation glide becomes the dominant source of strain. The mean dislocation velocity is then determined by the cutting of the dislocation network or other obstacles by the gliding dislocations. A general model for dislocation velocity in this case can be shown to be given by[9]:

$$v = \nu h_1 \sinh \left(\frac{(\sigma - \sigma_o - \sigma_1) b^2 h_2}{2kT} \right) \exp \left(\frac{-\sigma_2 b^2 h_2}{2kT} \right) \exp \left(\frac{-U_m}{kT} \right) . \tag{15}$$

This form of equation permits local forces on dislocations from their line tension on bowing out from pinning points or from pile-ups to be described. This would enable anelastic behaviour to be studied if the model were developed in that way. In this simplified treatment we will concentrate on the long range effect of the dislocation network and not differentiate between σ_1 and σ_2. For the case where the obstacles for dislocation movement are the other dislocations in the network the movement and pinning distances h_1 and h_2 are equated with the network size. The activation energy for cutting, U_m, is assumed to be twice the jog formation energy. The dislocation velocity is now:

$$v = \nu c_j^2 \frac{b^2}{\rho^{\frac{1}{2}}} \sinh \left[\frac{(\sigma - \sigma_o - \alpha \mu b \rho^{\frac{1}{2}})\Omega}{b \rho^{\frac{1}{2}} 2kT} \right] . \tag{16}$$

In this case the dislocations can move much further than one dislocation network spacing so equation (2) becomes:

$$\dot{\rho} = \beta \rho^{\frac{1}{2}} \frac{\dot{\varepsilon}}{b} - 2\rho^2 D_s \frac{b}{s} \frac{\mu\Omega}{kT} - \frac{\delta}{b} \rho \dot{\varepsilon} , \tag{17}$$

where β is inversely proportional to the distance it can move in units of the average network spacing. We will discuss the significance of below. Combining equations (1) and (16) together with equation (17) we now have a transient deformation model for stresses above the dislocation flow stress. The steady-state creep solution gives the following relationship between the applied stress and the dislocation density:

$$\sigma = \sigma_o + \alpha\mu b\rho^{\frac{1}{2}} + \frac{2kTb\rho^{\frac{1}{2}}}{\Omega} \sinh^{-1}\left(\frac{2 D_s \mu\Omega\rho}{\beta\nu s c_j bkT(1-\delta\rho^{\frac{1}{2}}/\beta)}\right) \quad (18)$$

The final term in equation (17) is negligible unless the dislocation density approaches the saturation limit $\rho=(\beta/\delta)^2$ in which case it becomes independent of the applied stress. In the lower end of the stress range when dynamic recovery is negligible the steady-state creep rate is given by:

$$\dot{\varepsilon} = \frac{2b^2\mu\Omega D_s}{skT}\left(\frac{\sigma-\sigma_o}{\alpha\mu b}\right)^3 . \quad (19)$$

When dynamic recovery dominates, at high stress, levels the steady-state creep rate becomes:

$$\dot{\varepsilon} = 2\nu c_j^2 \frac{b^3}{\delta} \sinh\left(\frac{(\sigma - \sigma_o - 2\mu b/\delta)\Omega\delta}{4\ bkT}\right) . \quad (20)$$

The overall dependence of creep strain rate on stress is illustrated in Fig.2. The four regimes are clearly seen in terms of the apparent stress power index. The Coble creep regime with its linear stress dependence is often not observed because the strain rates are very low, particularly when materials have large grain sizes and extensive precipitation on the grain boundaries. The climb-creep regime is often only seen at higher temperatures, again because the strain rates are low and practical creep tests are often only performed above the dislocation flow stress. The climb-recovery creep has an apparent stress index much higher than the value of 3 suggested by equation (18), because of the effect of the threshold stress. The sinh or exponential stress sensitivity is usually only observed in tests at lower temperatures, because of the associated very high creep rates and in initially well annealed material the primary creep strains which are less stress sensitive tend to be large.

4. The Behaviour of Stainless Steels

The models described above give clear indications of the expected relationship between applied stress and steady-state dislocation density. Fig.3 shows the observed dislocation densities for a range of stresses and temperatures on annealed 316 stainless steel[22-24]. Similar behaviour is shown by other austenitic stainless steels. This can be compared with the values predicted for the high and low stress models given in the previous section. The low stress data compares favourably with the low stress model for α=0.8. The high stress data of Morris and Harries is matched if a value of about 80MPa is taken for σ_o. The data of Challenger and Moteff might suggest a higher value of σ_o and that of Deleury et al a lower value. The flow stress is very sensitive to alloy composition and heat treatment so we might expect some degree of uncertainty. There is, however, clear evidence of a transition in mechanism.

In order to evaluate the models more fully a simple computer program was constructed which solved equations (1) and (2) as a function of time for conditions of either a fixed load or a fixed strain rate. The properties assumed for the calculation, given in Table 1, are for austenitic stainless steel with a composition similar to AISI 316 although no particular attempt was made to model this type of steel in detail. The size parameter s was taken to be the reciprocal of the jog concentration, c_j, and the value of δ was that given in equation (8). In order to model the behaviour of cold-worked steel the value of L was fixed at 10^{-7}m. The effectiveness of doing this will be seen and a justification will be given in the next section. The creep rate of the cold-worked material for the low stress model is:

$$\dot{\varepsilon} = \frac{2 D_s \Omega \mu}{b^2 skT} \frac{L}{} \left(\frac{\sigma}{(1 + \alpha)\mu} \right)^4 . \qquad (21)$$

A selection of data on steady-state creep of 316 type steels at 700°C are shown in Fig.5a[1,22,24-27]. The trends of the various blocks of data are indicated. Apart from an example of a linear stress sensitivity, which is a result of a particularly small grain size, the stress dependance of the creep rate is observed to be split into two regimes: a stress index n=3-4 for low stresses; and n=6-7 for high stresses. The various sets of data show less scatter at high stresses but creep rates differing by two orders of magnitude may be seen at lower stresses. The cold-worked material creeps at a rate which is an order of magnitude lower than the annealed material for most of the stress range. The rates tend to converge for very high stresses and the distinction becomes confused at low stresses. The results of our model calculations are shown in Fig.5b. The agreement between the observations and the model is encouragingly close and the main features of the observed creep rates are reproduced.

Examples of creep transients calculated by the model for cold-worked and annealed steel are shown in Fig.6. The results are typical of observations of primary creep for these conditions. The calculation for annealed steel shows the rapid decrease in the initial creep rate until the steady-state is established and the calculation for cold-worked steel shows the increase in creep rate as the cold-worked structure recovers.

The final example is for constant strain rate deformation. Fig.7 illustrates the development of hardening in cold-worked and annealed 316 steel at two temperatures. The results are very close to HEDL data collected under the same conditions[28].

5. Dislocation Immobilisation

In the previous section we have shown that our simple model has the potential for describing most features of high temperature deformation. However, a number of questions were left unresolved, i.e. the parameter β controlling the high temperature regime and reason for the distinction between cold-worked and annealed steel, when for a true steady-state solution they should be identical. In this section we will address these points but in order to do so it will be necessary to increase the complexity of the model.

Let us now consider two populations of dislocations; a mobile population with a density ρ_m and a population which is immobile with a density ρ_s. The deformation is produced by the mobile dislocation so:

$$\dot{\varepsilon} = b\rho_m v . \qquad (22)$$

We require a rate equation for each of the populations:

$$\dot{\rho}_m = \eta\rho_s^{\frac{1}{2}} v - \delta\rho_m (\rho_m + \rho_s) v - \rho_m \frac{v}{L} \qquad (23)$$

and

$$\dot{\rho}_s = \rho_m \frac{v}{L} - \delta\rho_m\rho_s v - 2 \frac{b}{s} D_s \rho_s^2 \frac{\mu\Omega}{kT} \qquad (24)$$

The main features of these equations are: (i) mobile dislocations are produced by the expansion of links of dislocation in the immobile network, of which a proportion, η, are very active; (ii) the dislocations move a distance L before being immobilised; (iii) dynamic recovery can take place either through mutual annihilation of mobile dislocations or by an interaction between a mobile and an immobile dislocation segment; and (iv) climb recovery occurs largely within the immobile network.

The climb recovery process holds the key to the understanding of the problem. The recovery takes two forms; dislocation segments can annihilate or

segments of the same Burger's vector can move into low energy configurations and form sub-boundary walls. These sub-boundaries provide the main obstacles to long range dislocation movement. In annealed material during monotonically loading we can equate the mean free path of the dislocation with the sub-grain diameter. Using equation (6) we get:

$$\rho_s^{\frac{1}{2}} = 1/(\beta d). \tag{25}$$

Let us take the steady-state limit for the low stress regime. From equation (23) and neglecting dynamic recovery we get:

$$\rho_m = \eta\rho_s/\beta , \tag{26}$$

and solving equation (22) and (24) for the case of climb creep we obtain:

$$\sigma = (\alpha + 1/\eta)\mu b\rho_s^{\frac{1}{2}} = (\alpha + 1/\eta)\mu b/\beta d . \tag{27}$$

In order for equation (25) to hold d must be inversely proportional to the applied stress. This is a widely observed relationship[22-25,29] which provides additional information to fix the unknown parameters. For 316 stainless steel the observed value of $(\alpha + 1/\eta)/\beta$ is approximately 20.

In the case of a cold-worked steel there is an initial high dislocation density. On heating the material to test temperature recovery reduces the dislocation density but many of the dislocations arising from cold-work become part of a sub-grain boundary structure. These sub-grains are very stable and persist during creep deformation unless recrystallisation takes place. The mean free path of the dislocations is thus limited to a value of:

$$L \sim 1/(\beta\rho_{cw}^{\frac{1}{2}}) , \tag{28}$$

where ρ_{cw} is the density of dislocations originally present from the cold-worked state. For steady-state creep the mobile dislocation density is given by:

$$\rho_m = \eta d\, \rho_s^{3/2} . \tag{29}$$

6. Sub-Grain Formation and Recrystallisation

In Section 5 we have given a solution to the problem of the mean free path of dislocations but we are left with questions on how sub-grain boundaries form and why they are so stable. A clue to the problem of sub-grain formation is given in a computer study by Holt[30]. A random distribution of dislocations with Burger's vectors of mixed signs, is found to re-distribute producing density fluctuations with a characteristic wavelength inversely proportional to the square root of the dislocation density. These density fluctuations form the nuclei for sub-boundaries. We might therefore anticipate that if the local dislocation density rises above the density associated with the existing sub-boundary dimensions then a new sub-boundary is nucleated. The observed relationship between sub-boundary size and applied stress is for this model the result of the dependence of dislocation density in the network on the applied stress.

Processes within the sub-boundary may be more important than implied by our simple model[31,32]. A schematic diagram of the interaction between dislocations and the sub-boundaries is shown in Fig.8. Dislocations reaching the boundaries are immobilised as the applied stress is not large enough for the dislocations to break through for creep conditions. The immobilised dislocations will be subjected to short range elastic interactions with the dislocations in the boundary which will cause them to climb into the boundary. Dislocations of the same sign as those making up the boundary will lose their long range elastic fields. Dislocations of opposite size will form dipoles within the boundary which are unstable against climb and will eventually be

eliminated. The presence of dipoles in the boundary is important as they may form sites for disloclation multiplication and still have a significant contribution to the internal stress field. The behaviour of dislocation in such a model will be dependent on the spacing of the dislocation and dipoles within the boundary. This results in a significantly more complicated set of rate equations. This model is discussed elsewhere[9].

The sub-boundaries formed during recovery of cold working appear to be very stable up to temperatures of 700°C. Above this temperature the material recrystallises after an incubation time which decreases with increasing temperature[33]. The recrystallisation is rapid but the temperature and incubation times for recrystallisation are very sensitive to the alloy composition and previous history. This stability of the sub-boundary structure is almost certainly due to the decoration of the sub-boundaries by precipitates. This mainly occurs during the initial recovery of the cold working at the temperatures of the mechanical tests. The recrystallisation is probably permitted by a coarsening of the precipitate concentration by a ripening process when the material is aged at high temperature. The recrystallisation starts by the growth of islands of low dislocation density, as the cold-worked structure tends to be inhomogeneous. Without the precipitates the sub-boundaries are apparently mobile for temperatures above 500°C, so the dynamics of precipitation are critical.

Recrystallisation is enhanced during creep, both the temperature for initiation and the incubation times are reduced[1]. One suggestion for for this is that creep increases the driving force for recrystallisation by increasing the dislocation density and hence the internal stress levels. There may be some contribution from this process, but the main effect is possibly from precipitation effects. New dislocations generated during deformation have been observed to nucleate precipitates and generally refine

the precipitate structure[22,24]. This secondary precipitation is very active and could deplete the sub-boundaries of precipitates and trigger recrystallisation. For a full understanding of high temperature deformation further work is required to develop a model for precipitation and recrystallisation.

After recrystallisation the cold-worked material is commonly observed to creep at the same rate as that seen in annealed material. However at low stress levels the creep rate may be higher than for annealed material with the same composition[1]. This is because primary recrystallisation often results in a reduction in grain size and a coarsening of the grain boundary precipitate size, permitting Coble creep.

7. The Effect of Irradiation

A full discussion of the effect of irradiation on high temperature deformation is outside the scope of this report, but it is worth looking at the implications of irradiation in the context of our simple model. It is well known that fast neutron irradiation can produce both hardening and softening effects in materials[34,35]. The production of small point defect clusters, interstitial loops, voids, helium bubbles and increasing the jogs concentration on dislocations all increase the effective flow stress. This is balanced by irradiation accelerating the ageing process in steels, coarsening the precipitate structure, which softens the material and accelerates recrystallisation in cold-worked materials. The greatest effects, however, are on the dislocation density. Well annealed materials show an increase in dislocation density and heavily cold-worked materials generally show a decrease. These both are manifested in changes in the strength of the material. For high displacement doses the dislocation density and the yield stress of the material tend to an equilibrium value, which is a weak function of dose rate and strong function of temperature.

The effect of irradiation on high temperature deformation is outside the scope of this report, but it is worth looking at the implications of irradiation in the context of our simple model by relating it to a forced climb-recovery velocity v_ϕ. Equation (2) is modified by adding radiation damage driven terms:

$$\dot{\rho} = \beta\rho^{\frac{1}{2}} \frac{\dot{\varepsilon}}{b} - 2\rho^2 \frac{b\mu\Omega}{s'kT} D_s - \frac{\delta'}{b} \rho \dot{\varepsilon}$$

$$+ v_\phi (c_1\rho^{3/2} - c_2\rho^{3/2} - \delta'\rho^2/b) . \qquad (30)$$

The quantities s and δ are given a dash to indicate that they will be changed by irradiation. The effect flwo stress of the dislocations, σ_o, will tend to increase which will reduce δ. The jog concentration on the dislocations will tend to increase decreasing the value of s', which will accelerate climb-recovery. The origin of the forced climb rate v_ϕ is an imbalance in the flux to the dislocations of vacancies and interstitials produced by displacement damage[6]. This can occur as a transient effect due to the higher mobility generally observed for interstitials over vacancies, but is more important as a continuing effect when there is accompanying void growth in the material. Here a higher flux of interstitials goes to dislocations because of a stronger elastic field interaction compared with vacancies. The supersaturation of vacancies must go to another sink, viz voids. In this case the forced climb rate is proportional to the swelling rate in the material and hence will have a complex dose dependence because of the effects of void nucleation and growth.

The first of the irradiation terms in equation (30) describe the multiplication of dislocations by the expansion of dislocation links by forced climb. This effect is described in the climb-creep model work[7]. It is balanced by the annihilation of dislocation dipoles in the network or

sub-boundaries by randomly orientated forced climb[34], represented by the second term. In general c_1 is greater than c_2 leading to an overall hardening effect from forced climb. The dislocation density is limited by dynamic recovery given by the final term. For high displacement dose rates at low temperatures dynamic recovery is an important process, as dislocation densities can be large. Even heavily cold-worked material can be further hardened at low temperatures.

If we neglect dynamic hardening from the deformation rate, which only occurs at high temperatures we obtain from equations (30) and (11) a relationship between applied stress and dislocation density during irradiation:

$$\sigma = (\alpha + 2/\beta - c_3) \rho^{\frac{1}{2}} + \sigma_\phi \qquad (31)$$

where

$$c_3 = \frac{v_\phi s'kT\delta'}{\beta b D_s \Omega\mu} \qquad (32)$$

and

$$\sigma_\phi = (c_1 - c_2) \frac{kTs'v_\phi}{D_s\Omega\beta} . \qquad (33)$$

The creep rate by dislocation climb, thermal and forced, is given by:

$$\dot{\varepsilon} = \left(\frac{2bD_s\Omega\mu}{\beta s'kT} + v_\phi \frac{\delta'}{\beta}\right) b \left(\frac{\sigma - \sigma_\phi}{(\alpha - c_3 + 2/\beta)\mu b}\right)^3$$

$$- v_\phi \frac{b}{\beta} (c_1 - c_2) \left(\frac{\sigma - \sigma_\phi}{(\alpha - c_3 + 2/\beta)\mu b}\right)^2 . \qquad (34)$$

The main points to note are that: there is a creep contribution from forced climb; and at high temperatures σ_ϕ is reduced enhancing the creep rate from both the thermal and forced climb processes. The expression for dislocation velocity is clearly inadequate for high dislocation densities and low stresses.

This model may provide some new insight into the interaction between thermal creep and irradiation. To be fully effective it requires coupling to a rate theory model of swelling for the forced climb velocity to be calculated.

8. Discussion and Conclusion

The simple dislocation model presented in this paper can reproduce many of the features of high temperature deformation of stainless steel. The fact that it has few unknown parameters and that these can be obtained from strain hardening measurements and the observed dislocation structure gives confidence that the model is a sound basis for a phenomenological treatment of transient creep.

The model also shows some promise for being extended into the range of irradiation behaviour. Depending on the choice of the parameters controlling the effect of irradiation in the model, irradiation can produce either an enhancement of the creep rate particularly at low stresses and high temperatures or a significant hardening at high stresses by increasing the dislocation flow stress. At lower temperatures pure irradiation creep is likely to mask any enhancement from forced climb recovery. A schematic illustration of the effect of irradiation is shown in Fig.9 for comparison with Fig.2.

In addition to the development of methods for calculating the effect of irradiation, further work is required on the effect of the microchemical state of materials. The development of precipitation and the coarsening of precipitation during ageing or irradiation needs to be understood. The role of deformation in affecting precipitation needs clarifying and the behaviour of solutes during these changes needs to be determined. The process of recrystallisation of cold-worked materials is important in nuclear applications because of the resulting softening and increase in creep rates, particularly at low stresses.

Acknowledgements

I would like to thank Dr. R. Bullough of Theoretical Physics Division at Harwell for his encouragement and advice. Other valuable suggestions were made by Dr. M. Finnis of Theoretical Physics Division and by Dr. T.M. Williams of Materials Development Division. Many of the ideas in this work arose from discussion with Professor F.R.N. Nabarro of the University of Witwatersrand.

References

1. J. Standring, A.M. Wilson and M.E. Clayden, 'Microstructural Instability and Thermal Creep in 20% Cold-Worked M316 Tubing', Proc. Conf. on Dimensional Stability of Irradiated Metals and Alloys, BNES Brighton, April 1983, paper 33, vol.2, p.79.

2. M.L. Hamilton et al, 'Mechanical Behaviour of Irradiated Fuel Pin Cladding Evaluated and Transient Heating and Pressure Conditions', ibid, paper 44, vol.1, p.211.

3. A.K. Miller and O.D. Sherby, 'Development of the Materials Code 'MATMOD', Electrical Power Research Institute report no. - EPRI-NP-567, Dec. 1977.

4. C.G. Schmidt and A.K. Miller, Res. Mechanica, 3(1981)109.

5. C.G. Schmidt and A.K. Miller, Res. Mechanica, 3(1981)175.

6. R. Bullough, ' Dislocations in Radiation Damage', Proc. Conf. on Dislocations and the Properties of Real Materials', Royal Society, London Dec. 1984, Cambridge University Press.

7. R. Bullough, M.W. Finnis and M.H. Wood, J. Nucl. Mater. 103 & 104(1981)1263.

8. R. Bullough, M.W. Finnis, J.R. Matthews and M.H. Wood, 'Progress in the Theory of Radiation and Thermal Creep', Proc. Conf. on Dimensional Stability of Irradiated Metals and Alloys, BNES Brighton, April 1983, paper 22, vol.1, p.25.

9. N. Gohniem and J.R. Matthews, to be published.

10. R.W. Bailey, J. Inst. Met. 35(1926)27.

11. E. Orowan, J. West Scotl. Iron & Steel Inst. 54(1946-7)45.

12. N.F. Mott, Phil. Mag. 44(1953)742.

13. R. Lagneborg, Int. Metal. Reviews, 17(1972)130.

14. J.H. Gittus, Phil. Mag., 21(1970)495 and 23(1971)1281.

15. W.G. Johnston and J.J. Gilman, J. Appl. Phys. 30(1959)129.

16. G.A. Webster, Phil. Mag. 14(1966)775.

17. U.F. Kocks, Trans ASME J. Eng. Mater. & Technology, 98(1976)76.

18. E. Voce, J. Inst. Metals, 74(1948)537.

19. J. Friedel, 'Les Dislocations', Gauthier-Villars, Paris 1956.

20. F.R.N. Nabarro, Phil. Mag. 16(1967)231.

21. A.H. Cottrell and M.A. Jaswon, Proc. Roy. Soc. A199(1949)104.

22. M.J. Deleury, J.R. Donati and J.L. Strudel, Ann. Chim. Fr., 6(1981)59.

22a. K.D. Challenger and J. Moteff, Met. Trans., 4(1973)749.

23. D.J. Michel, J. Moteff and A.J. Lovell, Met. Trans., 4(1973)1269.

24. D.G. Morris and D.R. Harries, 'Creep and Rupture in a Type 316 Stainless Steel at Temperature between 525°C and 900°C' Part-1 Creep Rate', Harwell Report AERE-R.8811, June 1977.

25. F. Garofalo et al, 'Strain-Time, Rate-Stress and Rate- Temperature Relations during Large Deformations in Creep', Joint International Conf. on Creep, Institution of Mechanical Engineers, Book 1, August 1963, paper 30, p.1.

26. Various unpublished AEA data on both cold-worked and annealed 316 steel.

27. A.J. Lovell, 'Creep of 20% CW Type 316 Stainless Steel', Hanford Report HEDL-TME 73-65, Oct. 1973.

28. M.M. Paxton, 'Mechanical Properties of Annealed and Cold-Worked 316 Stainless Steel Fast Reactor Seamless Tubing', Hanford Report HEDL-TME 74-11, Feb. 1974.

29. S. Takeuchi and A.S. Argon, J. Mater. Sci., 11(1976)1542.

30. D.L. Holt, J. Appl. Phys., 41(1970)3197.

31. A.S. Argon and S. Takeuchi, Acta. Met., 29(1981)1877.

32. F.R.N. Nabarro, R. Bullough and J.R. Matthews, Acta. Met., 30(1982)1761.

33. M.M. Paxton and J.J. Holmes, 'Recovery and Recrystallisation of Prototypic FTR Fuel Cladding - 20% CW 316 Stainless Steel Tubing', Hanford Report HEDL-TME 71-126, Oct. 1971.

34. J.R. Matthews, 'Deformation and Rupture Processes in Fuel Cladding Under Steady-State and Transient Reactor Conditions', Proc. Conf. on Irradiation Behaviour of Metallic Materials for Fast Reactor Core Components, Ajaccio, Corsica, June 1979, Vol.1, paper F1, p.272.

35. F.A. Garner et al, J. Nucl. Mater., 103 & 104(1981)803.

TABLE 1

Properties Used in Calculations

b(nm)	0.257
$\Omega(m^3)$	1.2×10^{-29}
$D_s(m^2\ s^{-1})$	$6 \times 10^{-5} \exp(-3.364 \times 10^4/T)$
μ(MPa)	$7.594 \times 10^4\ (1-3.413 \times 10^{-4}T)$
σ_ϕ(MPa)	$33.5 \exp(1250/T)$
c_j	$\exp(-\mu\Omega/5\pi kT)/b$
α	0.8
β(high stress range)	0.083
$\nu\ (s^{-1})$	10^{11}
L (cold-worked material)(m)	10^{-7}
Initial dislocation density (m^{-2})	
cold-worked	3×10^{14}
annealed	10^{11}

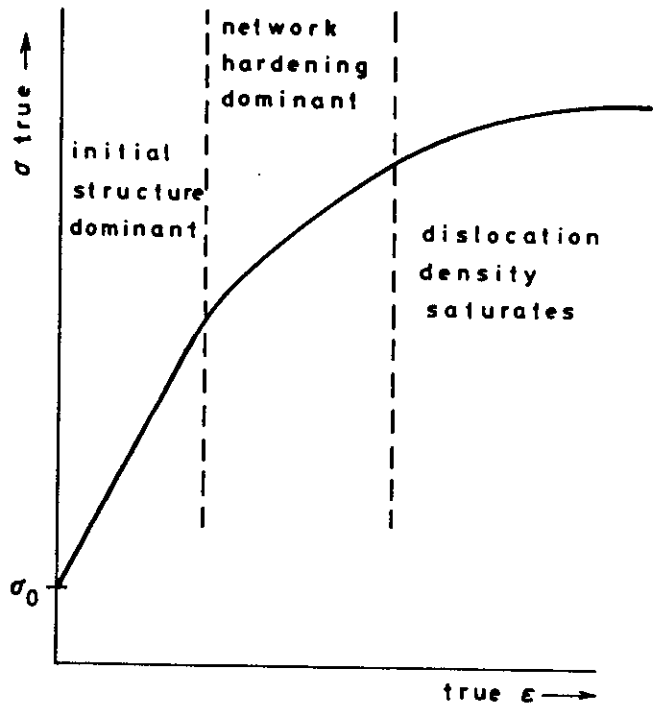

Fig. 1. The hardening regimes for low temperature or high strain rate deformation

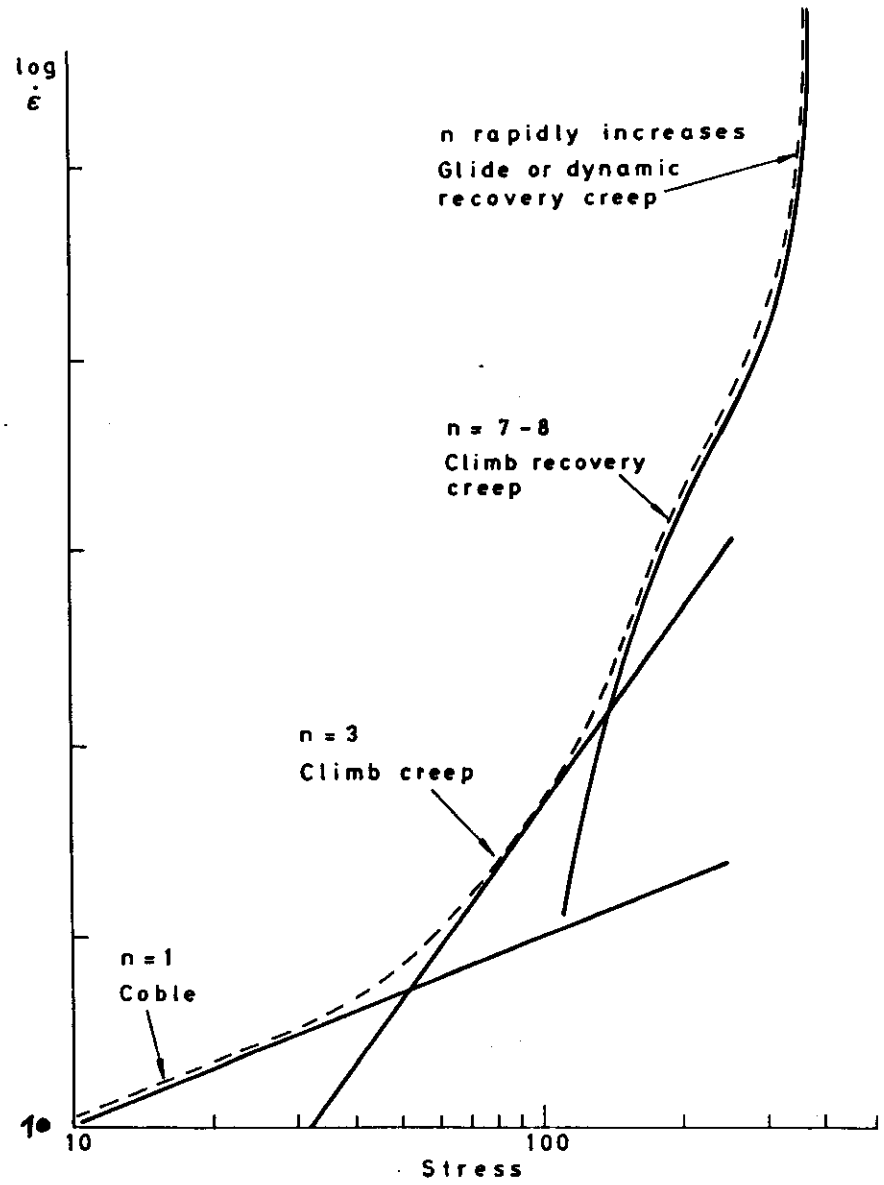

Fig.2. The transition between creep mechanisms for a function of applied stress

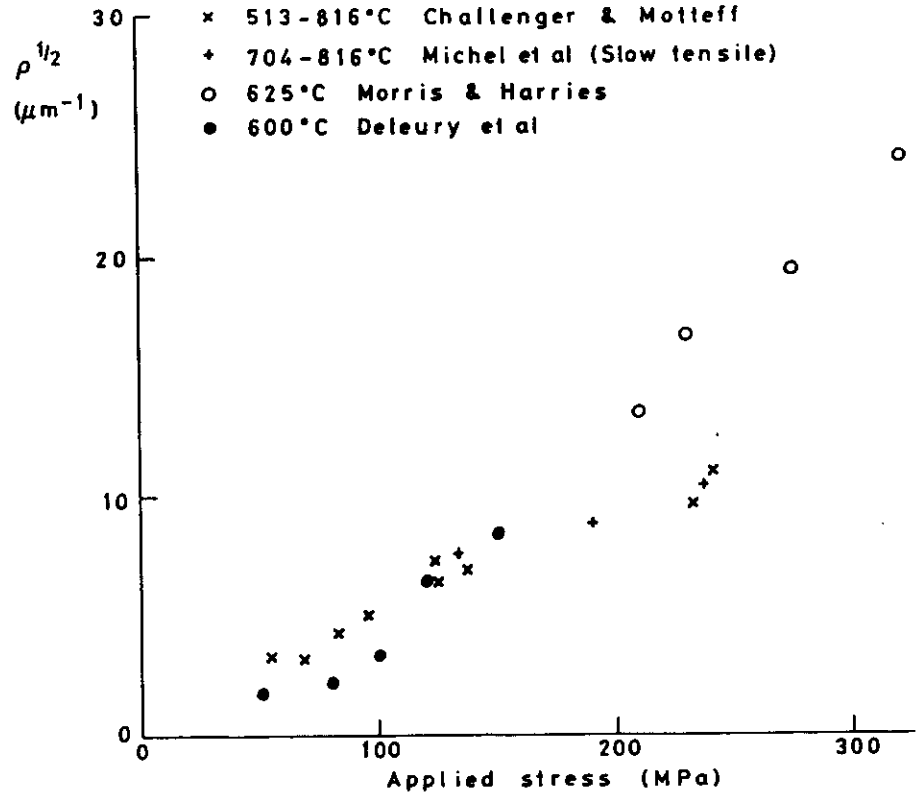

Fig.3. Observed relationship between dislocation density and applied stress for 316 steel

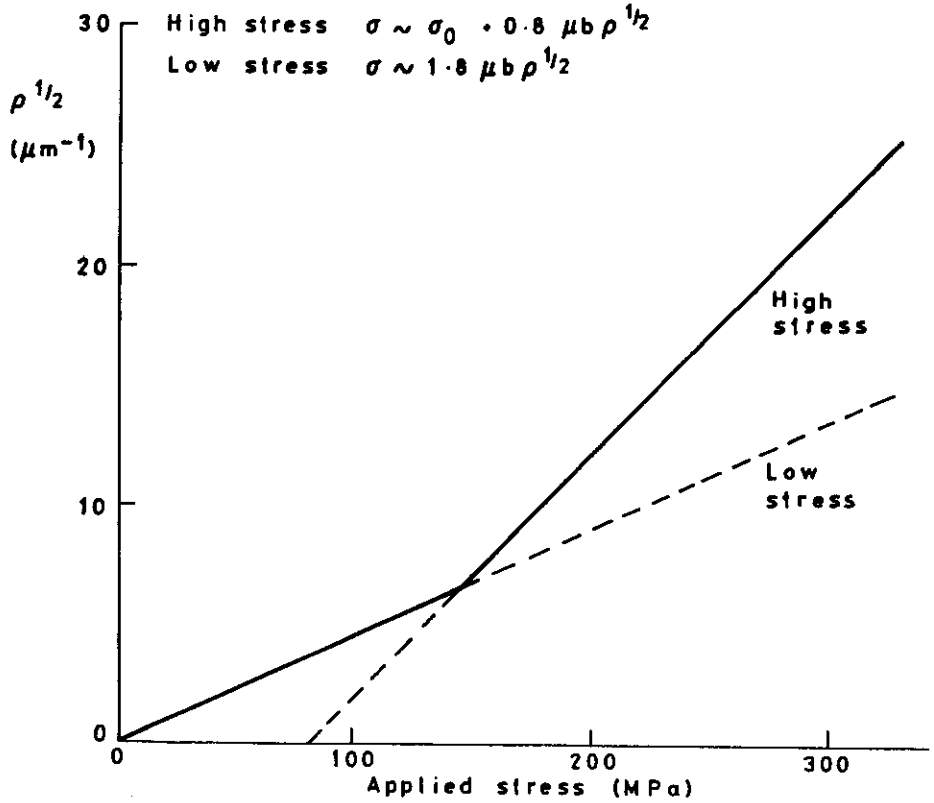

Fig. 4. Interpretation of dislocation density observations in terms of dislocation model

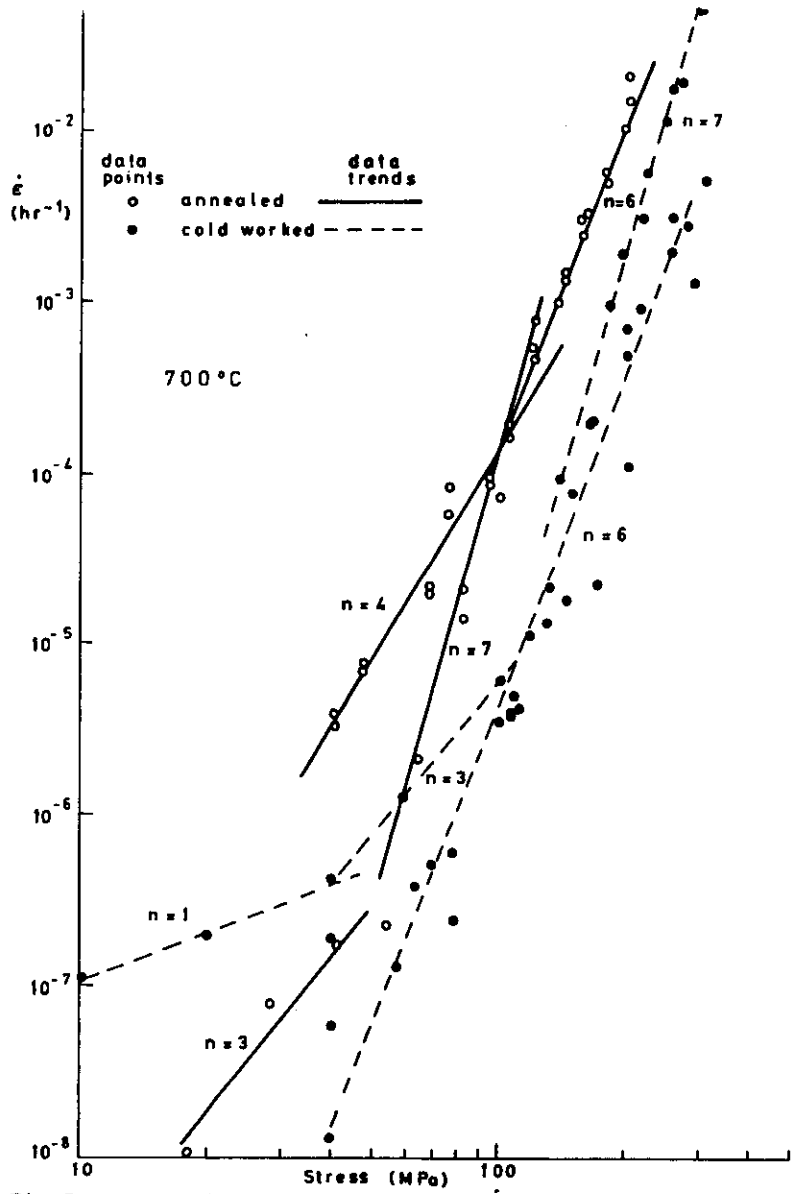

Fig. 5a. Comparison of the creep behaviour of cold worked and annealed 316 stainless steel

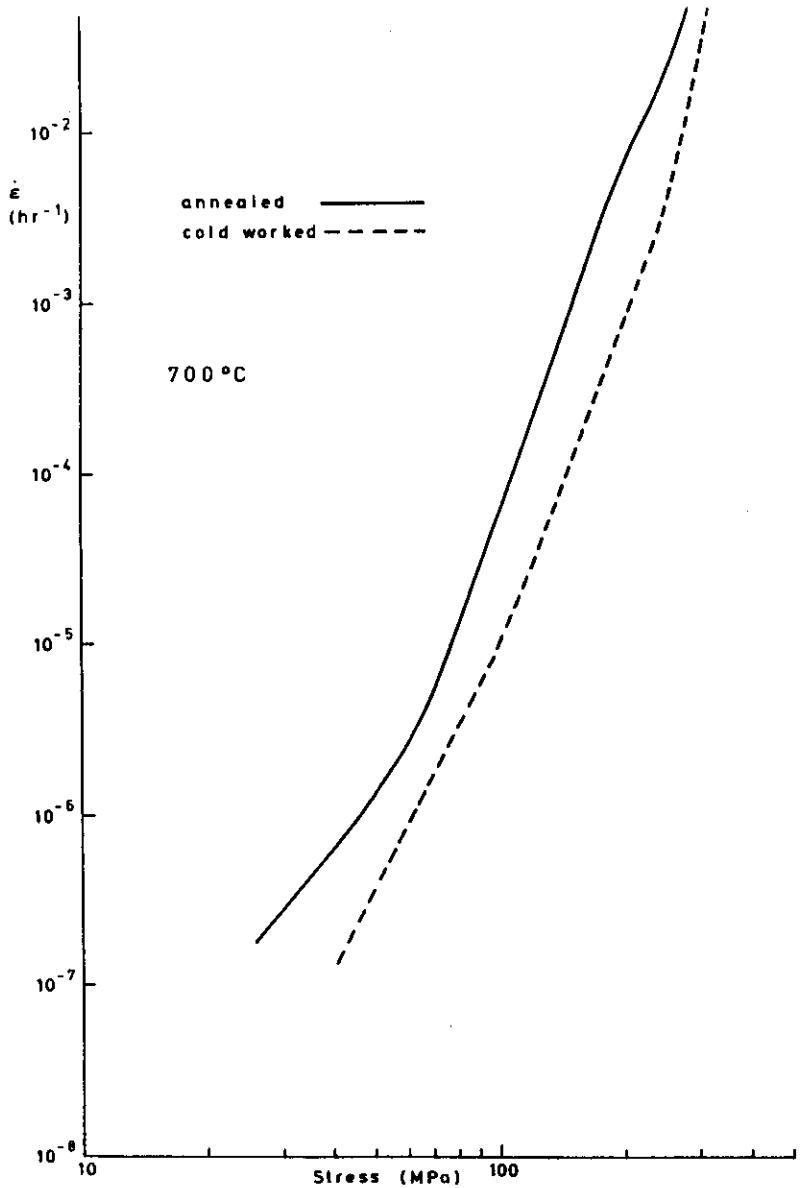

Fig. 5b. Calculated steady-state creep rates for cold worked and annealed 316 stainless steel.

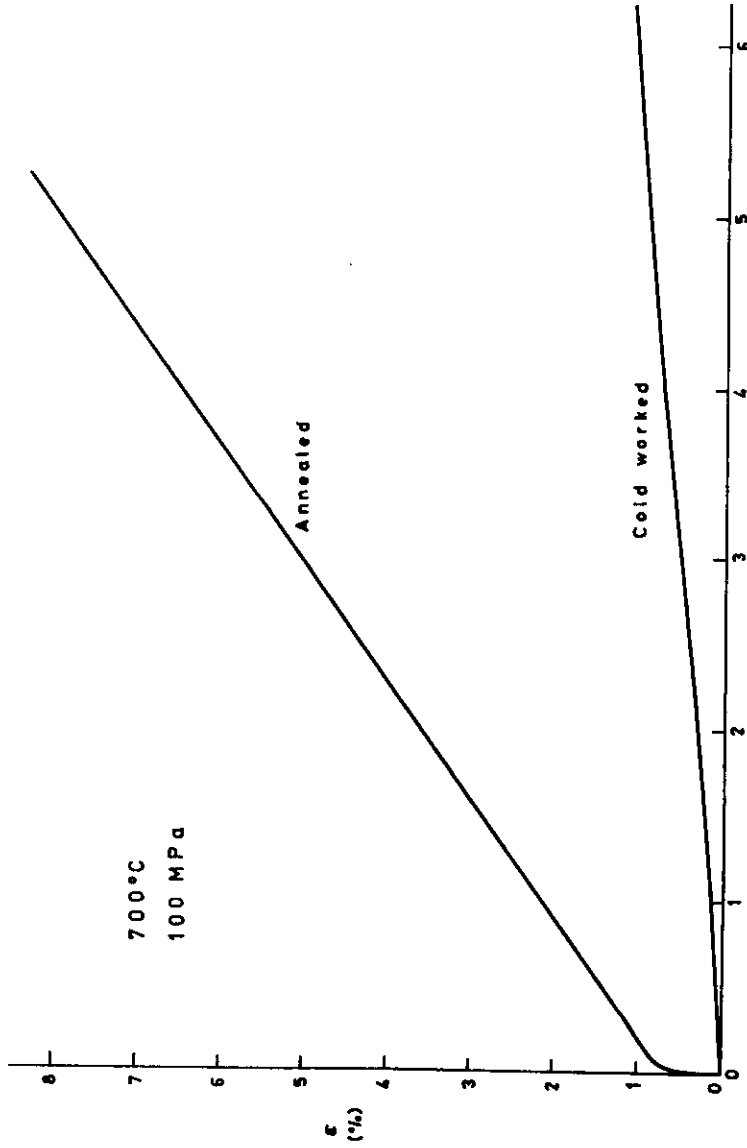

Fig. 6. Comparison of calculated creep transients for cold worked and annealed 316 steel

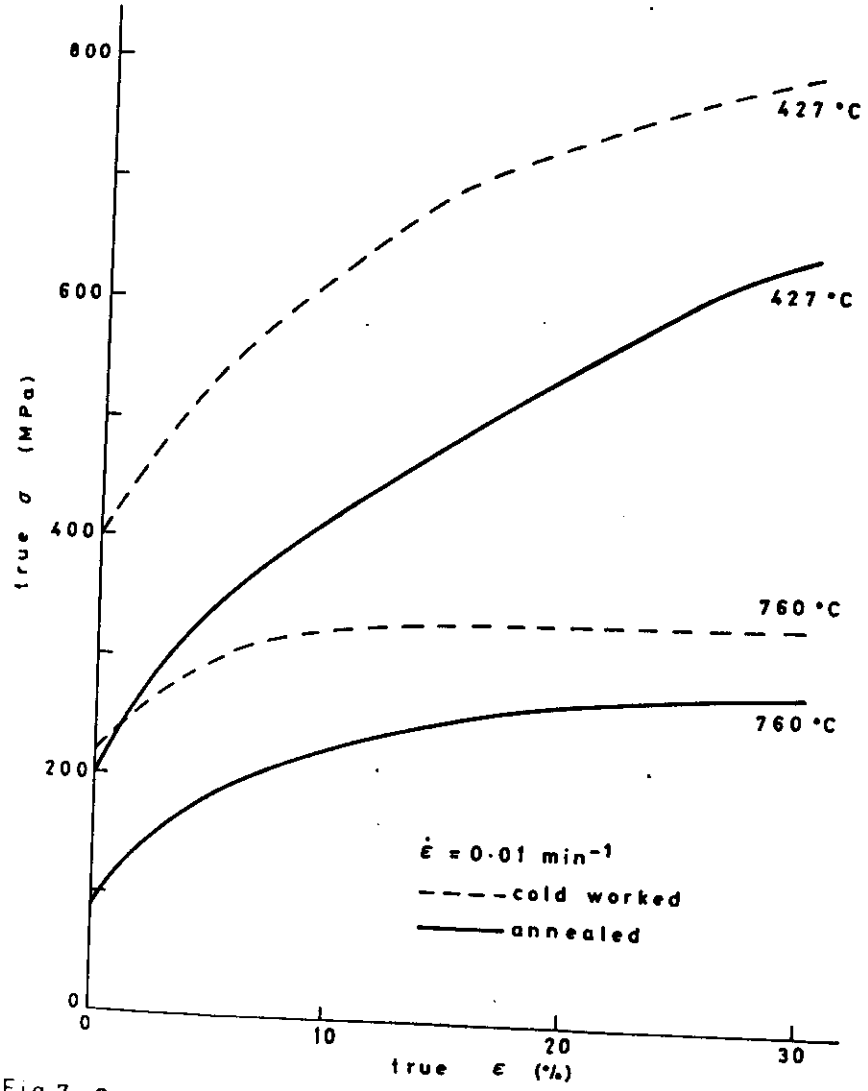

Fig. 7. Comparison constant strain rate stress-strain relationship for cold worked and annealed 316 steel

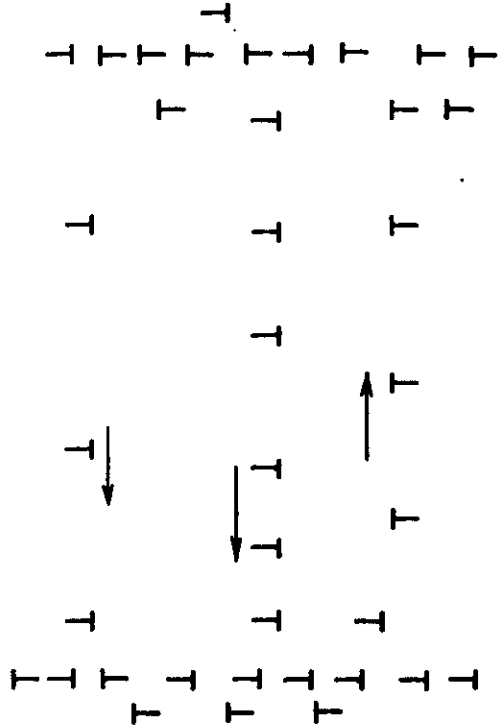

Fig. 8. Model for dislocation immobilisation at sub-boundaries

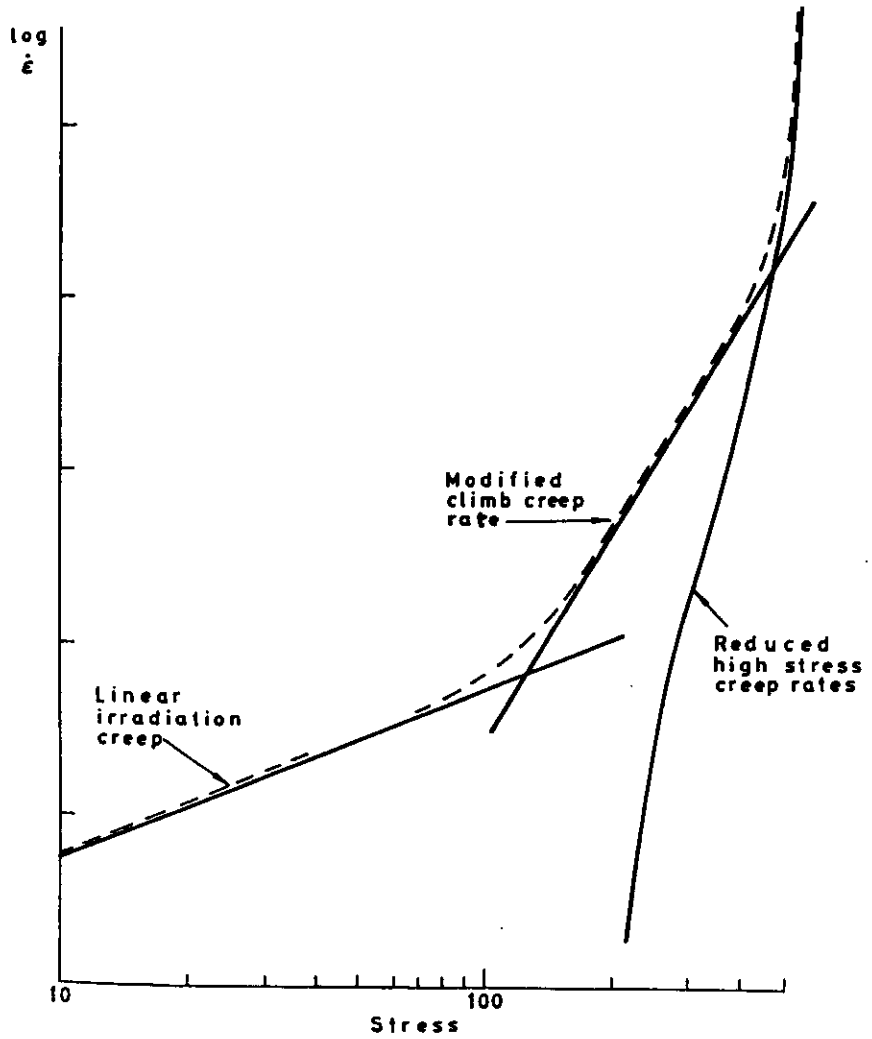

Fig. 9. Effect of irradiation on creep properties